International Journal of Computational Vision and Biomechanics
Vol. 3 No. 1 (January-June, 2017)

MUK PUBLICATIONS
Open Access Publisher

Segmentation of Carotid Artery Ultrasound Images Using Graph Cuts

Amr R. Abdel-Dayem[1] and Mahmoud R. El-Sakka[2]

[1]*Department of Mathematics and Computer Science, Laurentian University, Sudbury, Ontario, Canada*

[2]*Computer Science Department, University of Western Ontario, London, Ontario, Canada*

This paper proposes a scheme for segmenting carotid artery ultrasound images using graph cuts segmentation approach. Region homogeneity constraints, edge information and domain specific information are incorporated during the segmentation process. A graph with two terminals (source and sink) is formed by considering every pixel as a graph node. Each pair of neighbouring nodes is connected by a weighted edge, where the weight is set to a value proportional to the intensity of the gradient along them. Moreover, each graph node is connected to the source and the sink terminals with weights that reflect the confidence that the corresponding pixel belongs to the object and the background, respectively. The segmentation problem is solved by finding the minimum cut through the constructed graph. Experiments using a dataset comprised of 40 B-mode carotid artery ultrasound images demonstrates good segmentation results with (on average) 0.677 overlap with the gold standard images, 0.690 precision, and 0.983 sensitivity.

Keywords: *Carotid artery, morphology, graph theory, minimum cut, max flow.*

1. INTRODUCTION

According to the World Health Organization, there are over 20.5 million stroke cases worldwide, where 5.5 million of these cases are fatal. In Canada, approximately 16,000 Canadians die from stroke every year. Vascular plaque, a consequence of atherosclerosis, results in an accumulation of lipids, cholesterol, smooth muscle cells, calcifications and other tissues within the arterial wall. It reduces the blood flow within the artery and may completely block it. As plaque layers build up, it can become either stable or unstable. Unstable plaque layers in a carotid artery can be a life-threatening condition. If a plaque ruptures, small solid components (emboli) from the plaque may drift with the blood stream into the brain. This may cause a stroke. Early detection of unstable plaque plays an important role in preventing serious strokes.

Currently, carotid angiography is the standard diagnostic technique to detect carotid artery stenosis and the plaque morphology on artery walls. This technique involves injecting patients with a radio-active dye. Then, the carotid artery is examined using X-ray imaging. However, carotid angiography is an invasive technique. It is uncomfortable for patients and has some risk factors, including allergic reaction to the injected dye, renal failure, exposure to ionizing radiation, as well as arterial puncture site complications, e.g., pseudoaneurysm and arteriovenous fistula formation.

Ultrasound imaging provides an attractive tool for carotid artery examination. The main drawback of ultrasound imaging is the poor quality of the produced images. It takes considerable effort from clinicians to extract significant information about carotid artery contours and the possible existence of plaque layers that may exist. This task may require a highly skilled clinician. Furthermore, manual extraction of carotid artery contours generates a result that is not reproducible. Hence, a computer aided diagnostic (CAD) technique for segmenting carotid artery contours is highly needed.

Mao *et al*. [1] proposed a scheme for extracting the carotid artery walls from ultrasound images. The scheme uses a deformable model to approximate the artery wall. However, the result accuracy depends, to a large extent, on the appropriate estimation of the initial contour. Furthermore, the deformable model takes a considerable amount of time to approach the equilibrium state. It is worth mentioning that the equilibrium state of a deformable model does not guarantee the optimal state or contour shape.

Abolmaesumi *et al*. [2] proposed a scheme for tracking the center and the walls of the carotid artery in real-time. The scheme uses an improved star algorithm with temporal and spatial Kalman filters. The major drawback of this scheme is the estimation of the weight factors used by Kalman filters. In the proposed scheme, these factors are estimated from the probability distribution function of the boundary points. In practice, this distribution is usually unknown.

Da-chuan *et al*. [3] proposed a method for automatic detection of intimal and adventitial layers of the common carotid artery wall in ultrasound images using a snake model. The proposed method modified the Cohen's snake

[4] by adding spatial criteria to obtain the contour with a global maximum cost function. The proposed snake model was compared with the ziplock snake model [5] and was found to give superior performance. However, the computational time for the proposed model was significantly high. It took a long amount of time for the snake to reach the optimum shape.

Hamou *et al*. [6] proposed a segmentation scheme for carotid artery ultrasound images. The scheme is based on Canny edge detector [7]. The scheme requires three parameters. The first parameter is the standard deviation of the Gaussian smoothing kernel used to smooth the image before applying edge detection process. The second and the third parameters are upper and lower bound thresholds to mask out the insignificant edges from the generated edge map. The authors empirically tuned these parameters, based on their own database of images. This makes the proposed scheme cumbersome when used with images from different databases.

Abdel-Dayem *et al*. [8] proposed a scheme for carotid artery contour extraction. The proposed scheme uses a uniform quantizer to cluster image pixels into three major classes. These classes approximate the area inside the artery, the artery wall and the surrounding tissues. A morphological edge extractor is used to extract the edges between these three classes. The system incorporates a pre-processing stage to enhance the image quality and to reduce the effect of the speckle noise in ultrasound images. A post-processing stage is used to enhance the extracted contours. This scheme can accurately outline the carotid artery walls. However, it cannot differentiate between relevant objects with small intensity variations within the artery tissues. Moreover, it is more sensitive to noise.

Abdel-Dayem *et al*. [9] used the watershed segmentation scheme [10] to segment the carotid artery ultrasound images. Watershed segmentation schemes usually produce over-segmented images. Hence, a region merging stage is used to merge neighbouring regions based on the difference on their average pixel intensity. A single global threshold is needed during the region merging process. If this threshold is properly tuned, the proposed scheme produces accurate segmentation results.

Abdel-Dayem *et al*. [11] integrated multi-resolution-analysis with their watershed-based segmentation scheme [9] to reduce the computational cost of the segmentation process and at the same time reduce the sensitivity of the results with respect to noise. In this scheme, the image is decomposed into a pyramid of images at different resolutions using wavelet transform. Then, the lowest resolution image is segmented using Abdel-dayem *et al*. segmentation scheme [9]. Finally, the segmented image is projected back to produce the full resolution image.

Abdel-Dayem *et al*. [12] proposed a scheme for segmenting carotid artery ultrasound images using the fuzzy region growing technique. Starting from a user defined seed point within the artery; the scheme creates a fuzzy connectedness map for the image. Then, the fuzzy connectedness map is thresholded using an automatic threshold selection mechanism to segment the area inside the artery. The proposed scheme is a region-based scheme. Hence, it is resilient to noise. It produces accurate contours. This gain can be contributed to the fuzzy nature of objects within ultrasound images. Moreover, it is insensitive to the seed point location, as long as it is located inside the artery. However, the calculation of the fuzzy connectedness map is a computationally expensive process. To overcome this problem, Abdel-Dayem *et al.* [13] applied their fuzzy region growing scheme in multi-resolutions. In this configuration, the computational complexity is reduced as the fuzzy connectedness map is calculated for the lowest resolution image which has a size of $1/4^N$ of the original image size, where N is the number of decomposition levels.

Abdel-Dayem *et al*. [14] used the fuzzy c-means clustering algorithm to segment the carotid artery ultrasound images. In this scheme, the image pixels are clustered into three classes, representing the area inside the artery, the artery wall and the surrounding tissues. Local statistics, extracted from a 5×5 image block centred on every pixel, are employed during the clustering process. This scheme produces accurate contours in most cases. However, it sometimes fails due to the shadowing effect that may exist in ultrasound images.

The previous segmentation schemes are either region-based or edge-based. By integrating both region and edge information with domain specific information during the segmentation process, we hope that better segmentation results would be achieved. Graph-based segmentation schemes will be our vehicle to achieve such integration. This paper is an extension of our previous work [15] that uses graph cuts technique to segment carotid artery ultrasound images. More details and experimental results are included in this paper.

It is worth mentioning that, there are other various research directions that deal with carotid artery ultrasound images. One of these directions incorporates artificial intelligence systems to examine plaque layers over carotid artery walls [16] [17]. Another research direction is based on fluid dynamic-based systems. They use blood velocity and pressure to estimate the elasticity of the carotid artery walls [18] [19] or calculating the shear stress in carotid arteries [20] [21]. Other techniques [22] [23] try to estimate the arterial wall velocity using Doppler ultrasound images. However, these directions are outside the scope of our research, which is image processing-based systems only.

The rest of this paper is organized as follows. Section 2 describes the graph cuts segmentation approach. Section 3 describes the proposed scheme in details. Section 4 presents the results. Finally, Section 5 offers the conclusions of this paper.

2. IMAGE SEGMENTATION VIA GRAPH CUTS

Image segmentation can be formulated as an energy minimization problem. The minimization of such an energy function corresponds to partitioning image pixels into object and background segments. Several optimization techniques can be used to minimize such energy function [24] [25] [26] [27]. The success of the graph cuts based segmentation schemes can be attributed to the combination of both region and edge information during the segmentation process. The region information forces the homogeneity of the segmented area. Meanwhile, the incorporation of the edge information prevents the *leak* (i.e. overgrowth of the segmented region) that generally appears in most region-based segmentation schemes.

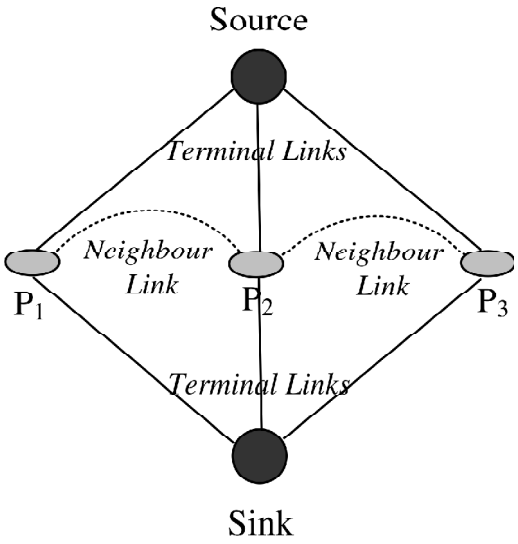

Figure 1: A Graph Constructed for a Three-pixel Image

In order to segment an image, a weighted graph is created, in which, each node in the graph corresponds to an image pixel. Two special terminal nodes are added to the graph, namely: source node and sink node, representing the object and the background segments, respectively. All non-terminal graph nodes (i.e., image pixels) are connected to the source and the sink nodes with edges referred to as *terminal-links*. Neighbouring nodes are connected by weighted edges called *neighbour-links*. Figure 1 shows a graph constructed for an image with three pixels.

A cut on the graph is defined as a subset of graph edges that separate the source from the sink node. The cost of a cut is the summation of its edge weights. The image is segmented by finding the minimum cost cut on the graph. The minimum cut problem can be solved using various standard algorithms from combinatorial optimization. These algorithms can be classified into two major classes, the *push-relabel* [28][29] and the *augmenting paths* [30] [31] [32] [33] [34] [35]. In this paper we used Boykov *et al*. algorithm [35] due to its efficient execution time. The speed up in this algorithm is achieved by building two search trees, one from the source and the other from the sink. Then, the algorithm tries to reuse these trees and never start building them from scratch. The major drawback of this algorithm is that the produced cut is not necessarily the optimum one. However, this approximation is acceptable in most image processing applications.

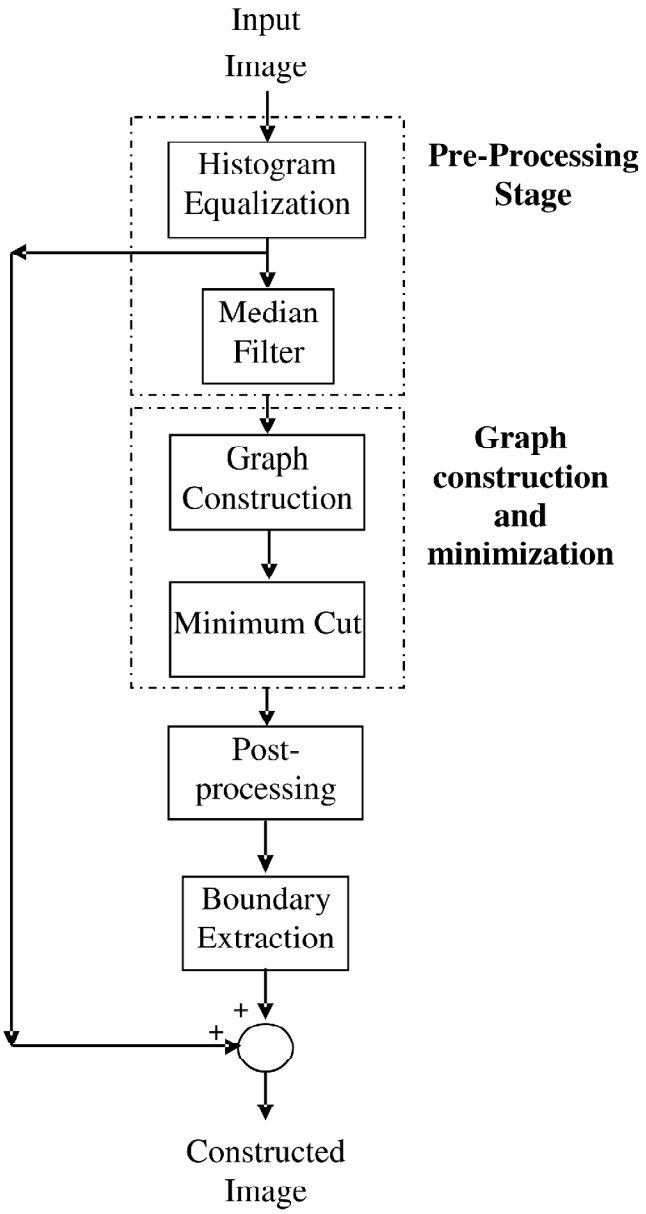

Figure 2: The Block Diagram of the Proposed Scheme

3. THE PROPOSED SOLUTION

The proposed scheme consists of four major stages. These stages are: (1) pre-processing, (2) graph construction and minimum cut finding, (3) post-processing, and (4) boundary extraction. Figure 2 shows the block diagram of the proposed method. In the following subsections, a detailed description of each stage is introduced.

3.1. Pre-processing Stage

Ultrasound images suffer from several drawbacks. One of these drawbacks is that ultrasound images have relatively low contrast. Another severe problem is the presence of random speckle noises, caused by the interference of the reflected ultrasound waves. These factors severely degrade any automated processing and analysis of the images. Hence, it is crucial to enhance the image quality prior to any further processing. In this stage we try to overcome these problems by performing two pre-processing steps. The first is a histogram equalization step [36] to increase the dynamic range of the image gray levels. In the second step, the histogram equalized image is filtered using a median filter to reduce the amount of the speckle noise in the image. It was empirically found that a 3×3 median filter is suitable for the removal of most of the speckle noise without affecting the quality of the edges in the image.

3.2. Graph Construction and Minimum Cut Finding

In this stage, the pre-processed image is segmented using graph cuts-based segmentation approach, described in Section 2. First, a two terminal weighted graph is constructed for the image under consideration. Second, the weights of terminal-links and neighbour-links are set. Finally, the minimum cut through the graph is generated using Boykov *et al*. algorithm [35]. Graph nodes that remain connected to the source node represent object pixels, whereas nodes connected to the sink node represent background pixels.

The weight of a *terminal-link* is set to a value that reflects our confidence that the given pixel belongs to either the object or the background. Due to the nature of the carotid artery ultrasound images, the area inside the artery (which is the object of interest) is darker than the rest of the image. Hence, pixels with intensities less than a certain object threshold μ_{object} are connected by terminal links to both source and sink nodes with weights equal to one and zero, respectively. Meanwhile, pixels with intensities greater than a background threshold $\mu_{background}$ are connected by terminal links to the source and sink nodes with weights equal to zero and one, respectively. This way, the domain specific information is considered. All other nodes are connected to source and sink nodes with links that have certain weights. A terminal link weight (for a given node) is calculated by a non-negative decreasing function of the absolute differences between the node's intensity and the object and the background thresholds, μ_{object}, $\mu_{background}$, respectively (this represents a region homogeneity constraint). In the proposed scheme we used an exponential function to calculate the *terminal-link* weights, as described in Equation (1) and Equation (2).

$$W_{P,Source} = \begin{cases} 1 & if \quad I_P \le \mu_{object} \\ 0 & if \quad I_P \ge \mu_{background} \\ e^{-\left(\frac{I_P - \mu_{object}}{\alpha}\right)^2} & otherwise \end{cases} \tag{1}$$

and,

$$W_{P,Sink} = \begin{cases} 0 & if \quad I_P \le \mu_{object} \\ 1 & if \quad I_P \ge \mu_{background} \\ e^{-\left(\frac{I_P - \mu_{background}}{\alpha}\right)^2} & otherwise \end{cases} \tag{2}$$

where, $W_{P,Source}$ and $W_{P,Sink}$ are the weights of the *terminal-link* connecting node P to the *source* and the *sink* nodes, respectively. I_P is the intensity of pixel P. μ_{object} and $\mu_{background}$ are the object and the background thresholds, respectively. α is a regulating term, used to control the rate of decay for the exponential weight function. This regulating term allows the weight function to cope up with the fuzzy (or defused) boundaries of the objects within the ultrasound images. We empirically set μ_{object} and $\mu_{background}$ to 10% of the lower and higher intensity

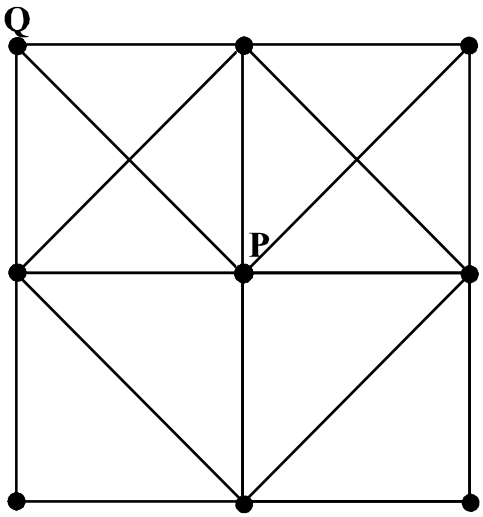

Figure 3: The 8-connectivity Neighbourhood System, used to Calculate the *Neighbour Link Weight* between Points P and Q

ranges, respectively. Whereas a is set to 2% of the total intensity range. Hence, for 8-bit images, we set μ_{object} to 25, $\mu_{background}$ to 230 and a to 5. Note that, in ultrasound images, the object of interest appears darker than the background.

We used the 8-connectivity neighbourhood system, as shown in Figure 3, to assign the *neighbour-link* weights. These weights are set based on local gradients according to Equation (3),

$$W_{P,Q} = e^{-\left(\frac{I_P - I_Q}{\sigma}\right)^2}, \quad (3)$$

where, $W_{P,Q}$ is the weight of the *neighbour-link* connecting nodes P and Q, I_P and I_Q are the intensities of pixels P and Q, respectively, and s is the standard deviation of the gradient magnitude through the image. Note that *neighbour-link* weights represent the edge information.

By finding the minimum cut through the graph edges, a binary image, which separates the object from the background, is formed. The extracted object contains the area inside the carotid artery and some dark objects that usually exist in a given ultrasound image. The user can specify a seed point within the artery to extract the artery wall and neglect all other objects which are outside the region of interest.

3.3. Post-processing Stage

The objective of this stage is to smooth the edges of the segmented area and to fill any gaps or holes that may present due to the presence of noise in ultrasound images. Hence, we used a morphological opening operation [36] [37] with a rounded square structuring element of size W. The size of the structuring element can be adjusted, based on the maximum gap size in the segmented area, according to Equation (4),

$$W = (h \times 2) + 1, \quad (4)$$

where, W is the size of the structuring element and h is the maximum gap size that exists in the segmented image. We empirically found that generally, the maximum gap size does not exceed two pixels. Hence we used a 5×5 structuring element.

3.4. Boundary Extraction Stage

The objective of this stage is to extract the boundaries of the segmented regions. Various edge detection schemes can be used for this purpose [36]. In our system, we use a morphological-based contour extraction mechanism [36], [37]. First, the image produced by the previous stage is morphologically eroded using a 3×3 rounded square structuring element. Then, the eroded image is subtracted from the non-eroded image to obtain the boundary of the segmented region, which represents the artery wall. This operation can be described by Equation (5),

$$\text{Boundary}\ (A) = A - (A\ \theta\ B),$$

where, A is the post-processed image, B is the structuring element and θ is the erosion operator. Finally, the extracted contour is superimposed on the histogram equalized image to produce the final output of the proposed scheme.

4. RESULTS

Our proposed system was tested using a set of 40 B-mode ultrasound images. These images were obtained using ultrasound acquisition system (Ultramark 9 HDI US machine and L10-5 linear array transducer) and were digitized with a video frame grabber. These images were carefully inspected by an experienced clinician and artery contours were manually highlighted to represent gold standard images. These gold standard images are used to validate the results produced by our proposed systems.

We used the image shown in Figure 4 to demonstrate the output produced by our proposed system. This image is a typical carotid artery ultrasound image, where the arterial lumen is complicated by speckle noise. Figure 5(a) shows the output after the histogram equalization step, while Figure 5(b) shows the histogram of the image shown in Figure 5(a). Comparing the two histograms shown in Figure 4(b) and Figure 5(b) reveals that the histogram equalization step increases the dynamic range and the contrast of the image. Unfortunately, the histogram equalization step increases the speckle noise that exists in ultrasound images. However, the next step in the pre-processing stage will compensate for this drawback. Figure 6 shows the image produced by applying a 3×3 median filter to the histogram equalized image shown in Figure 5(a). This image represents the output from the pre-processing stage. In order to show the importance of applying the median filter, in Figure 7, we magnify the area inside the artery *region of interest* before and after this step. Comparing Figure 7(a) and Figure 7(b) reveals that the amount of noise within the artery is reduced. This noise reduction step has great impact in the accuracy of the segmentation results during the following stages of the proposed scheme.

Figure 8(a) shows the segmented area produced by applying the minimum cut of the graph constructed from the pre-processed image shown in Figure 6. The image contains some objects that are outside the region of interest. Figure 8(b) shows the image shown in Figure 8(a) after applying a morphological opening operation using a 5×5 rounded square structuring element (the post-processing stage). Comparing Figure 8(a) and Figure 8(b) demonstrates the importance of the post-processing in filling any gaps and smoothing the boundaries of the segmented area.

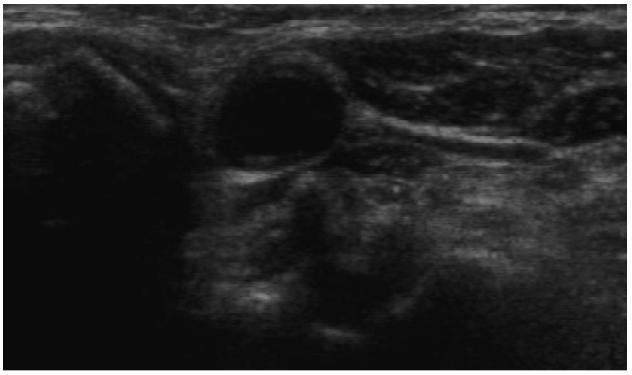

(a)

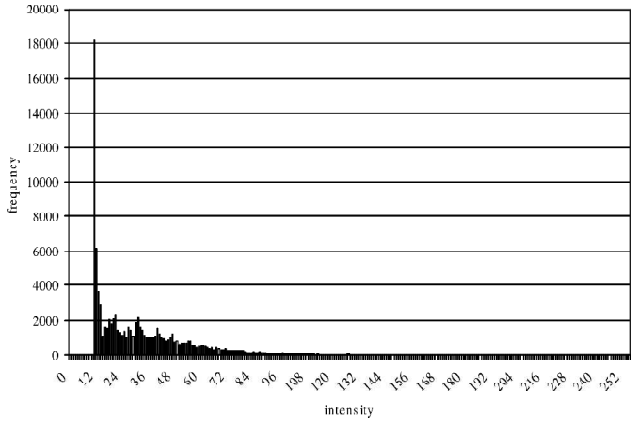

(b)

Figure 4: (a) The Original Carotid Artery Ultrasound Image, (b) the Histogram of the Image Shown in (a)

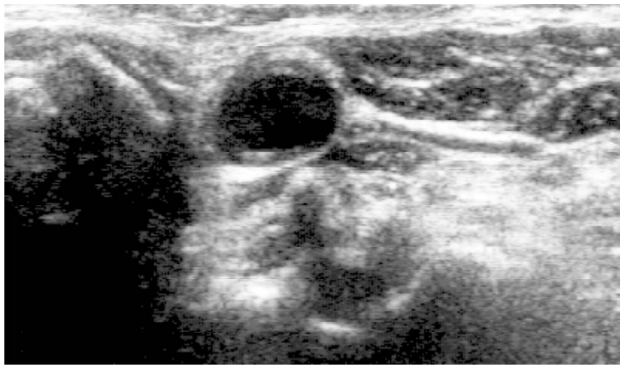

(a)

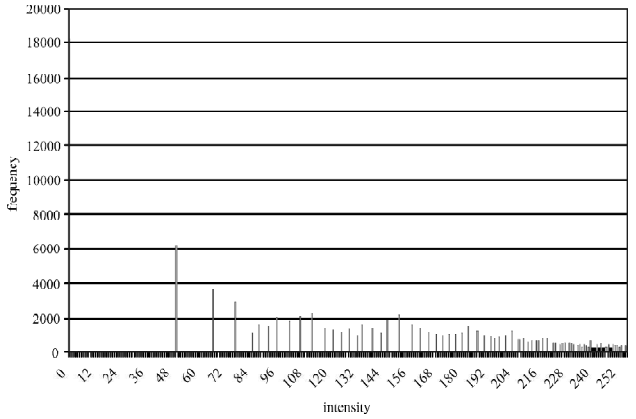

(b)

Figure 5: (a)The Image Shown in Figure 4(a) After Applying the Histogram Equalization Step, (b) the Histogram of the Image Shown in(a)

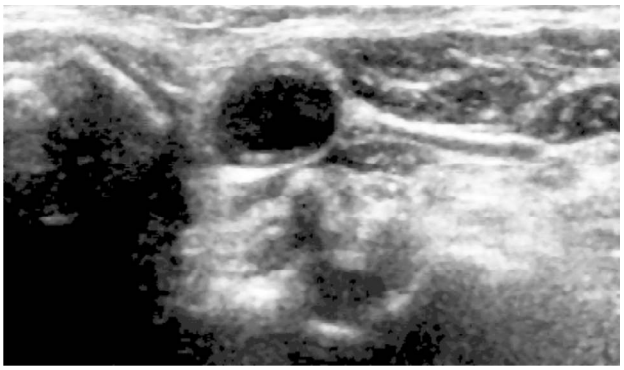

Figure 6: The Histogram Equalized Image Shown in Figure 5 after Applying a 3×3 Median Filter

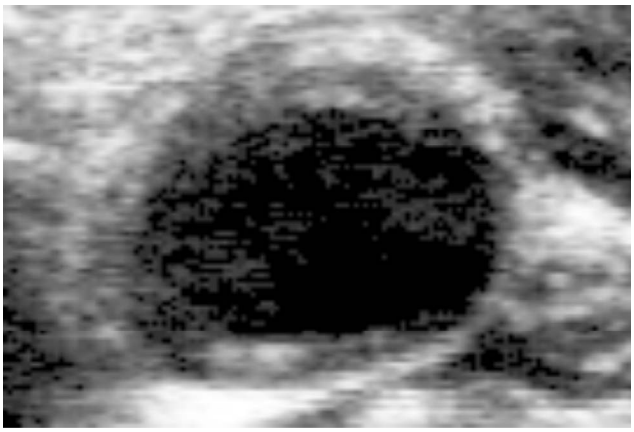

(a)

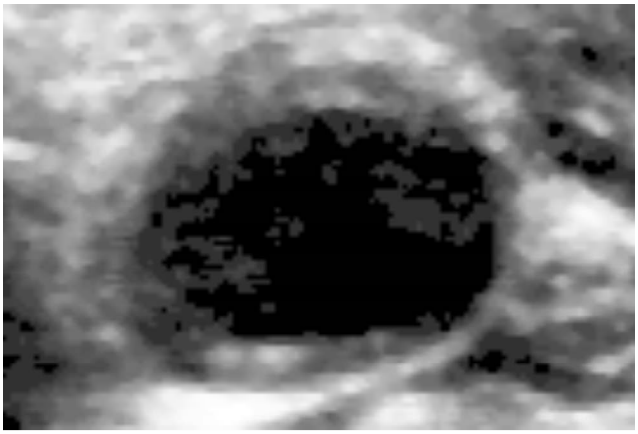

(b)

Figure 7: (a) The region of interest in the histogram equalized image, (b) the ROI after the noise removal step

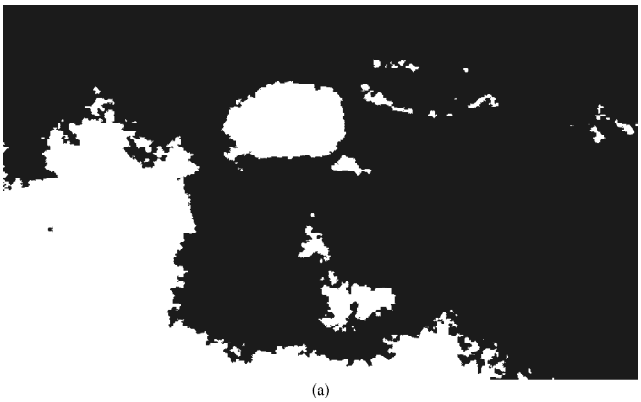

(a)

(b)

Figure 8: (a) The Segmented Image Produced by Applying the Minimum Cut Algorithm, (b) the Image Shown in (a) After Applying a Morphological Opening Operation using a 5×5 Rounded Square Structuring Element. This is the Output Produced by the Post-processing Step

Figure 9(a) shows the boundary of the segmented area. This image represents the output of the contour extraction stage. Finally, Figure 9(b) shows the final output of the proposed scheme, where the extracted contour is superimposed on the histogram equalized image. By selecting a seed point within the artery, the proposed scheme can extract the region of interest, while neglecting all other components. This result is shown in Figure 10. Figure 11 shows the gold standard image (the artery contour is manually highlighted by an experienced clinician) for same test case, shown in Figure 10. The subjective comparison between Figure 10 and Figure 11 showed that the proposed scheme produces accurate artery contour.

To demonstrate the contribution of the *neighbour-link* weights in the final segmentation results, Figure 12 shows The output of the proposed scheme when only the *terminal-link* weights are active (hard constraints). The comparison between Figure 10 and Figure 12 reveals that the incorporation of the *neighbour-link* weights improves the segmentation results, as they tend to hang neighbouring pixels together to produce meaningful objects.

To evaluate the performance of the proposed scheme, we objectively compared it with our recent three schemes [11][13][14]. The comparison results are presented in Section 4.1.

4.1. Objective Analysis

The results produced by the proposed system (for the entire set of fifty images) were objectively compared to the gold standard images (the clinician segmented images). Three different performance measures were used in the comparison. These measures are the overlap ratio, precision, and sensitivity. Figure 13 shows the definition of the *true positive* (*TP*), *false positive* (*FP*), *true negative* (*TN*) and *false negative* (*FN*) terms. Equations (6), (7)

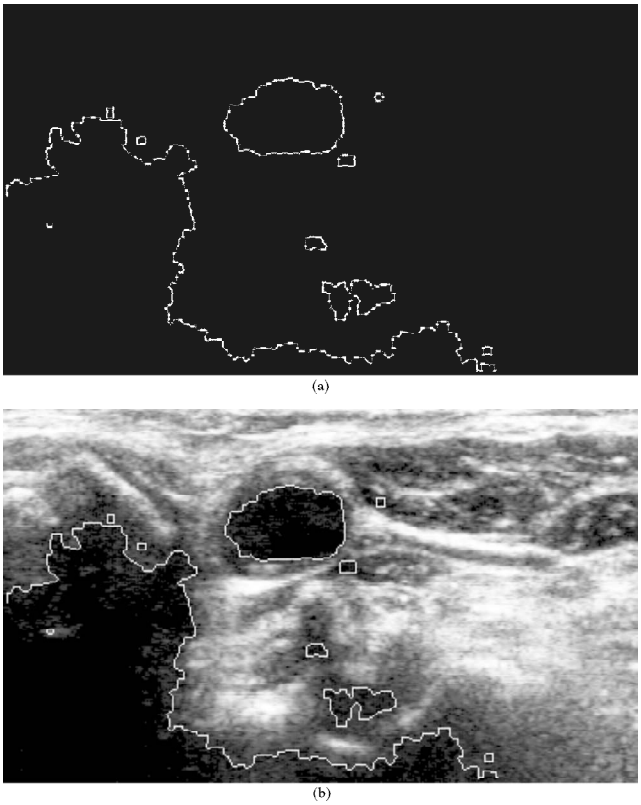

(a)

(b)

Figure 9: (a) The Boundary of the Segmented Area. This is the Output from the Contour Extraction Stage, (b) the Final Output (the Histogram Equalized Image with the Carotid Artery Contour Highlighted)

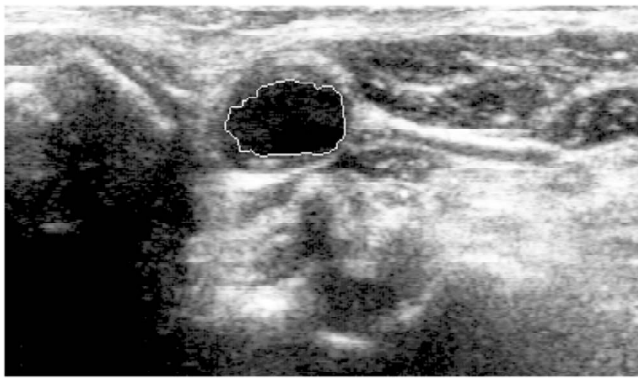

Figure 10: The Output of the Proposed Scheme when the user Specifies a Seed Point within the Artery Area

Figure 11: The Gold Standard Image, where the Artery Contour is Highlighted by an Experienced Clinician

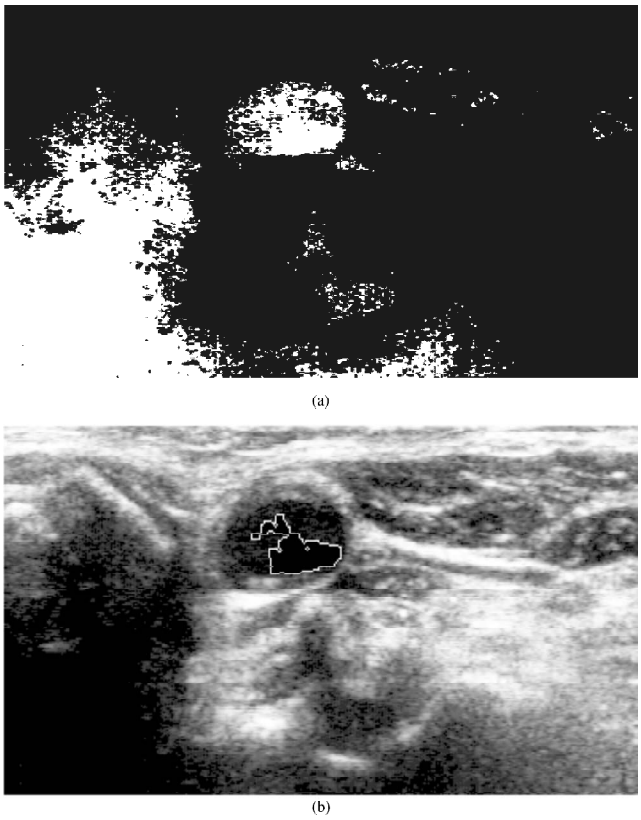

Figure 12: (a) The Segmented Image Due to the Hard Constraint Only, (b) the Final Output of the Proposed Scheme when only the Hard Constraints are Applied

and (8) show the definition of the overlap ratio, the precision and the sensitivity, respectively:

$$Overlap\ \ ratio = \frac{TP}{FN + TP + FP} \tag{6}$$

$$Precision = \frac{TP}{TP + FP} \tag{7}$$

and

$$Sensitivity = \frac{TP}{TP + FN} \tag{8}$$

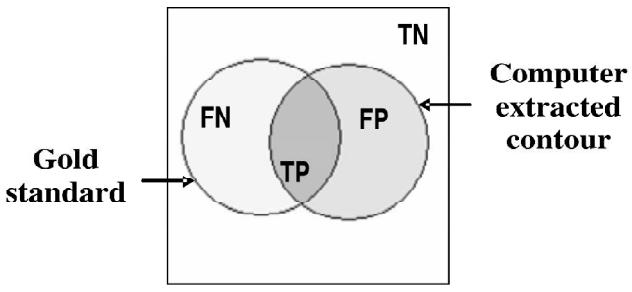

Figure 13: The Definition of the *True Positive* (TP), *False Positive* (FP), *True Negative* (TN) and *False Negative* (FN) Terms, used to Calculate the *Overlap Ratio*, the *Precision* and the *Sensitivity*

The objective analysis over the entire set of 40 test images revealed that on average the proposed scheme produces an overlap ratio of 0.677, a precision of 0.690 and a sensitivity of 0.983. Table 1 summarizes the performance of the proposed system over the entire set of images. Table 2 through Table 4 show the corresponding values for fuzzy c-means scheme [14], multi-resolution and fuzzy region growing scheme [13], and multi-resolution and watershed scheme [11], respectively.

The comparison between Table 1 and Table 2 through Table 4, as well as Figure 14, Figure 15, and Figure 16 shows that the proposed scheme improves both the overlap ratio and the precision measures. However, the sensitivity remains within approximately the same range. It is worth mentioning that the proposed system as well as the systems presented in [11], [13] and [14] tend to overestimate the artery contour. As a result of this, they have a tendency to produce higher values for the sensitivity measure. Currently, we attempt to collect more comprehensive and challenging images for further experimentation.

Table 1
Performance Measures of the Proposed Scheme over 40 Test Images

	Overlap ratio	*Precision*	*Sensitivity*
Average	0.677	0.690	0.983
Standard deviation	0.147	0.161	0.023
95% confidence interval	[0.632, 0.722]	[0.640, 0.739]	[0.976, 0.990]

Table 2
Performance Measures of Fuzzy c-means Scheme [14] over 40 Test Images

	Overlap ratio	*Precision*	*Sensitivity*
Average	0.655	0.663	0.986
Standard deviation	0.152	0.161	0.016
95% confidence interval	[0.608, 0.702]	[0.614, 0.713]	[0.982, 0.991]

Table 3
Performance Measures of Multi-resolution and Fuzzy Region Growing Scheme [13] over 40 Test Images

	Overlap ratio	*Precision*	*Sensitivity*
Average	0.584	0.588	0.992
Standard deviation	0.159	0.164	0.010
95% confidence interval	[0.534, 0.633]	[0.537, 0.639]	[0.989,0.995]

Table 4
Performance Measures of Multi-resolution and Watershed Scheme [11] over 40 Test Images

	Overlap ratio	*Precision*	*Sensitivity*
Average	0.662	0.677	0.976
Standard deviation	0.140	0.154	0.029
95% confidence interval	[0.618, 0.705]	[0.629, 0.724]	[0.967, 0.985]

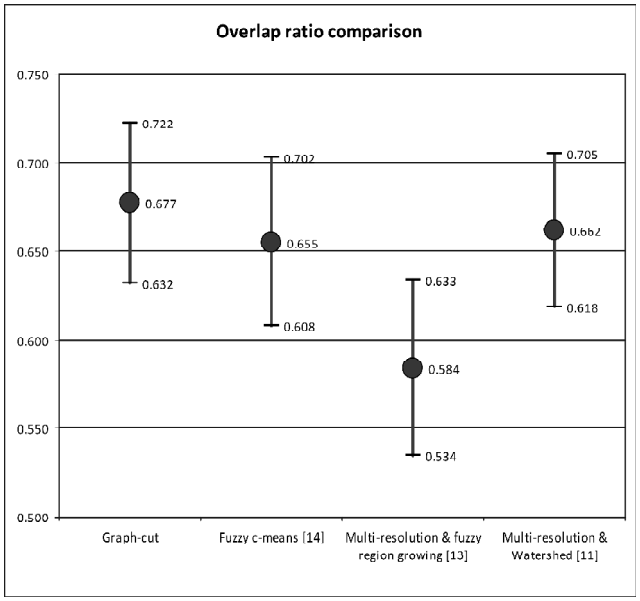

Figure 14: The 95% Confidence Interval of the Overlap Ratio Produced by the Proposed Graph-cut Scheme, Fuzzy c-means Scheme [14], Multi-resolution and Fuzzy Region Growing Scheme [13], and Multi-resolution and Watershed Scheme [11]

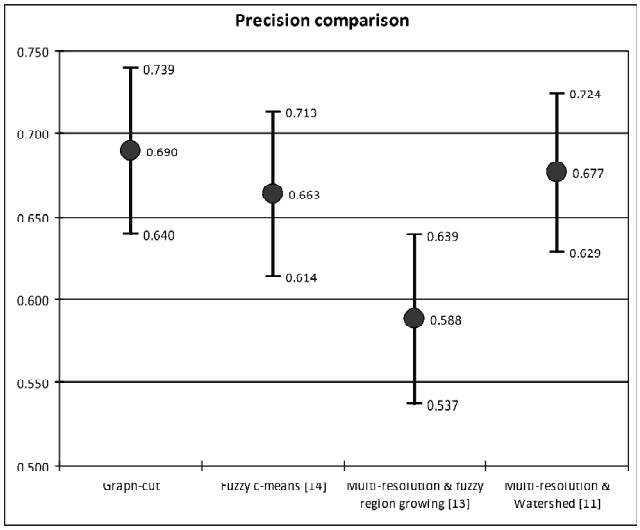

Figure 15: The 95% Confidence Interval of the Precision Measure Produced by the Proposed Graph-cut Scheme, Fuzzy c-means Scheme [14], Multi-resolution and Fuzzy Region Growing Scheme [13], and Multi-resolution and Watershed Scheme [11]

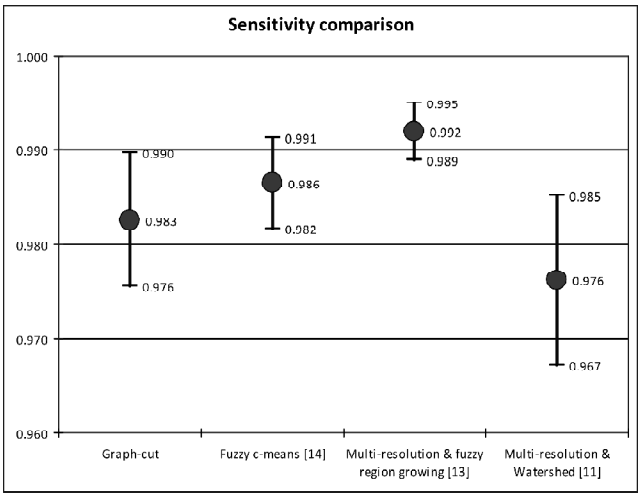

Figure 16: The 95% Confidence Interval of the Sensitivity Measure Produced by the Proposed Graph-cut Scheme, Fuzzy c-means Scheme [14], Multi-resolution and Fuzzy Region Growing Scheme [13], and Multi-resolution and Watershed Scheme [11]

5. CONCLUSION

In this paper, we proposed a novel scheme for highlighting the carotid artery contour in ultrasound images. The proposed scheme is based on using a graph cut approach to segment the image. The graph weights are formed in terms of both local intensity gradients (edge feature), as well as, penalty weights to assign every pixel to either object or background areas (region feature). Then, the image is segmented by finding the minimum cut through the graph. Experimental results over a set of sample images showed that the proposed scheme provides a good estimation of carotid artery contours.

ACKNOWLEDGEMENTS

This research is partially funded by the Natural Sciences and Engineering Research Council of Canada (NSERC). This support is greatly appreciated. The authors would like to thank The Robarts Research Institute at the University of Western Ontario for providing us with the ultrasound images that were used to test the proposed scheme.

REFERENCES

[1] F. Mao, J. Gill, D. Downey, and A. Fenster, "Segmentation of Carotid Artery in Ultrasound Images", *Proceedings of the 22nd IEEE Annual International Conference on Engineering in Medicine and Biology Society*, 3: 1734–1737, 2000.

[2] P. Abolmaesumi, M. Sirouspour, and S. Salcudean, "Real-time Extraction of Carotid Artery Contours from Ultrasound Images", *Proceedings of the 13th IEEE Symposium on Computer-Based Medical Systems*, pp. 81–186, 2000.

[3] C. Da-chuan, A. Schmidt-Trucksass, C. Kuo-Sheng, M. Sandrock, P. Qin, and H. Burkhardt, "Automatic Detection of the Intimal and the Adventitial Layers of the Common Carotid Artery Wall in Ultrasound B-mode Images using Snakes", *Proceedings of the International Conference on Image Analysis and Processing*, pp. 452–457, 1999.

[4] L. Cohen, "On Active Contour Models and Balloons", *Computer Vision, Graphics, and Image Processing: Image Understanding*, 53(2): 211–218, 1991.

[5] W. Neuenschwander, P. Fua, L. Iverson, G. Szekely, and O. Kubler, "Ziplock Snake", *International Journal of Computer Vision*, 25(3): 191–201, 1997.

[6] A. Hamou and M. El-Sakka, "A Novel Segmentation Technique for Carotid Ultrasound Images", *Proceedings of the IEEE International Conference on Acoustics, Speech and Signal Processing*, 3: 521–424, 2004.

[7] J. Canny, "Computational Approach to Edge Detection", *IEEE Transactions on Pattern Analysis and Machine Intelligence*, 8(6): 679–698, 1986.

[8] A. Abdel-Dayem and M. El-Sakka, "A Novel Morphological-based Carotid Artery Contour Extraction", *Proceedings of the Canadian Conference on Electrical and Computer Engineering*, 2: 1873–1876, 2004.

[9] A. Abdel-Dayem, M. El-Sakka, and A. Fenster, "Watershed Segmentation for Carotid Artery Ultrasound Images", *Proceedings of the IEEE International Conference on Computer Systems and Applications*, pp. 131–138, 2005.

[10] L. Vincent and P. Soille, "Watersheds in Digital Spaces: An Efficient Algorithm Based on Immersion Simulations", *IEEE Transactions on Pattern Analysis and Machine Intelligence*, 13(6): 583–598, 1991.

[11] A. Abdel-Dayem and M. El-Sakka, "Carotid Artery Contour Extraction from Ultrasound Images using Multi-resolution-Analysis and Watershed Segmentation Scheme", *ICGST International Journal on Graphics, Vision and Image Processing*, 5(9): 1–10, 2005.

[12] A. Abdel-Dayem and M. El-Sakka, "Carotid Artery Ultrasound Image Segmentation using Fuzzy Region Growing", Proceedings of the International Conference on Image Analysis and Recognition, ICIAR 2005, LNCS 3656, pp. 869–878, Springer-Verlag Berlin Heidelberg, September 2005.

[13] A. Abdel-Dayem and M. El-Sakka, "Multi-resolution Segmentation using Fuzzy Region Growing for Carotid Artery Ultrasound Images", *Proceedings of the IEEE International Computer Engineering Conference*, 8 pages, 2006.

[14] A. Abdel-Dayem and M. El-Sakka, "Fuzzy c-means Clustering for Segmenting Carotid Artery Ultrasound Images", Proceedings of the International Conference on Image Analysis and Recognition, ICIAR 2007 pp. 933–948, Springer-Verlag Berlin Heidelberg, August 2007.

[15] A. Abdel-Dayem and M. El-Sakka, "Graph-based Segmentation for Carotid Artery Ultrasound Images", *Proceedings of the International Conference on Computational Vision and Medical Image Processing*, VIP Image 2007, pp. 275–279.

[16] P. Theocharakis, I. Kalatzis, N. Piliouras, N. Dimitropoulos, and D. Cavouras, "Computer based Analysis of Ultrasound Images for Assessing Carotid Artery Plaque Risk", *Proceedings of the 3rd International Symposium on Image and Signal Processing and Analysis ISPA* 2003, 2: 717–721, 2003.

[17] S. Mougiakakou, S. Golemati, I. Gousias, K. Nikita, and A. Nicolaides, "Computer-aided Diagnosis of Carotid Atherosclerosis using Laws' Texture Features and a Hybrid Trained Neural Network", *Proceedings of the 25th Annual International Conference of Engineering in Medicine and Biology Society*, 2: 1248–1251, 2003.

[18] H. Hasegawa, H. Kanai, and Y. Koiwa, "Detection of Lumen-intima Interface of Posterior Wall for Measurement of Elasticity of the Human Carotid Artery", *IEEE Transactions on Ultrasonics, Ferroelectrics and Frequency Control*, 51(1): 93 –108, 2004.

[19] Z. Xiaoming, R. Kinnick, M. Fatemi, and J. Greenleaf, "Noninvasive Method for Estimation of Complex Elastic Modulus of Arterial Vessels", *IEEE Transactions on Ultrasonics, Ferroelectrics and Frequency Control*, 52(4): 642 –652, 2005.

[20] F. Glor, B. Ariff, A. Hughes, L. Crowe, P. Verdonck, D. Barratt, S. Thom, D. Firmin, and X. Xu, "The Integration of Medical Imaging and Computational Fluid Dynamics for Measuring Wall Shear Stress in Carotid Arteries", *Proceedings of the 26th Annual International Conference of the Engineering in Medicine and Biology Society, EMBC*, 1: 1415–1418, 2004.

[21] G. Bambi, T. Morganti, S. Ricci, F. Guldi, and P. Tortoli, "Real-time Simultaneous Assessment of Wall Distension and Wall Shear Rate in Carotid Arteries", *IEEE Ultrasonics Symposium*, 1: 592–595, 2004.

[22] D. Adam, and D. Givorry, "Estimation of Flow Velocity Vectorial Profile by Ultrasound Color Doppler Mapping", Proceedings of the 19th Annual International Conference of the IEEE on Engineering in Medicine and Biology Society, 2: 829–831, 1997.

[23] P. Tortoli, R. Bettarini, F. Guidi, F. Andreuccetti, and D. Righi, "A Simplified Approach for Real-time Detection of Arterial Wall Velocity and Distension", *IEEE Transactions on Ultrasonics, Ferroelectrics and Frequency Control*, 48(4): 1005–1012, 2001.

[24] R. Horst, P. Pardalos, and N. Thoai, "Introduction to Global Optimization", Dordrecht; Boston: Kluwer Academic Publishers, 1995.

[25] E. Chong and S. Zak, "An Introduction to Optimization", New York: Wiley, 1996.

[26] P. Adby and M. Dempster, "Introduction to Optimization Methods", London: Chapman and Hall; New York: Halsted Press, 1974.

[27] G. Reklaitis, A. Ravindran and K. Ragsdell, "Engineering Optimization: Methods and Applications", New York; Toronto: Wiley, 1983.

[28] B. Cherkassky and A. Goldberg, "On Implementing Push-relabel Method for the Maximum Flow Problem", *Algorithmica*, 19: 390–410, 1997.

[29] A. Goldberg and R. Tarjan, "A New Approach to the Maximum-flow Problem", *Journal of the Association for Computing Machinery*, 35(4): 921–940, 1988.

[30] L. Ford and D. Fulkerson, "Flows in Networks", Princeton University Press, 1962.

[31] E. Dinic, "Algorithm for Solution of a Problem of Maximum Flow in Networks with Power Estimation", Soviet Math. Dokl, 11: 1277–1280, 1970.

[32] J. Edmonds and R. Karp, "Theoretical Improvements in Algorithmic Efficiency for Network Flow Problems", *ACM Journal*, 19(2): 248–264, 1972.

[33] Z. Galil and A. Naamad, "An O (EV log2V) Algorithm for the Maximal Flow Problem", *Journal of Computer and System Sciences*, 2(1): 203–217, 1980.

[34] H. Gabow, "Scaling Algorithms for Network Problems", *Journal of Computer and System Sciences*, 31(2): 148–168, 1983.

[35] Y. Boykov and V. Kolmogorov, "An Experimental Comparison of Min-cut/max-flow Algorithms for Energy Minimization in Vision", *IEEE transactions on Pattern Analysis and Machine Intelligence*, 26(9): 1124–1137, 2004.

[36] G. Gonzalez and E. Woods, "Digital Image Processing", Second Edition, Prentice Hall, 2002.

[37] E. Dargherty and R. Lotufo, "Hands–on Morphological Image Processing", The Society of Photo-Optical Instrumentation Engineers, 2003.